

EVIDENCE FOR NEUTRINO OSCILLATION FROM SUPER-KAMIOKANDE

R. Jeffrey Wilkes

*Department of Physics, University of Washington
Seattle, Washington, USA*

(For the Super-Kamiokande Collaboration[1])

Abstract

Two independent data samples from a 33.0 kiloton-year (535-day) exposure of the Super-Kamiokande detector provide mutually consistent evidence for neutrino oscillations. The atmospheric neutrino data exhibit a zenith angle dependent deficit of muon neutrinos which is inconsistent with expectation based on accepted calculations of the atmospheric neutrino flux. Experimental biases and uncertainties in the prediction of neutrino fluxes and cross sections are unable to explain these observations. The data are consistent with two-flavor $\nu_\mu \leftrightarrow \nu_\tau$ oscillations with $\sin^2 2\theta > 0.82$ and $5 \times 10^{-4} < \Delta m^2 < 6 \times 10^{-3} \text{ eV}^2$ at 90% confidence level. Upward-going stopping and through-going neutrino-induced muon fluxes have also been measured. The through-going upward muon flux and the ratio of stopping to through-going fluxes as a function of zenith angle both deviate significantly from expectation based on the absence of neutrino oscillations, while they agree with expectation assuming two-flavor $\nu_\mu \leftrightarrow \nu_\tau$ oscillations. The values of $\sin^2 2\theta$ and Δm^2 obtained from the upward muon data are consistent with those obtained from the Super-K atmospheric neutrino data.

1 Introduction

Super-Kamiokande has found evidence for neutrino oscillations in two independent data samples: atmospheric neutrino interactions within the detector, and observations of upward-going muons, where the neutrino interaction vertex is below the detector. Results presented here represent analysis of 33.0 kiloton-years (535 live-days) of atmospheric neutrino data from Super-Kamiokande. This paper includes some results not available at the time of the conference, and others which may have already been presented elsewhere[2, 3, 4].

Atmospheric neutrinos are produced as decay products of hadronic secondaries from collisions of cosmic rays with nuclei in the upper atmosphere. Production of electron and muon neutrinos is dominated by the processes $\pi^+ \rightarrow \mu^+ + \nu_\mu$ followed by $\mu^+ \rightarrow e^+ + \bar{\nu}_\mu + \nu_e$ (and their charge conjugates) giving an expected ratio ($\equiv \nu_\mu/\nu_e$) of the flux of $\nu_\mu + \bar{\nu}_\mu$ to the flux of $\nu_e + \bar{\nu}_e$ of about two. Calculations of the absolute neutrino fluxes have uncertainties on the order of 20%. The ν_μ/ν_e ratio, in which common uncertainties cancel, has been calculated in detail with an uncertainty of less than 5% over a broad range of energies from 0.1 GeV to 10 GeV [5, 6]. Measurements are reported in terms of the “ratio of ratios”, $R \equiv (\mu/e)_{DATA}/(\mu/e)_{MC}$, where μ and e are the number of muon-like (μ -like) and electron-like (e -like) events observed in the detector for both data and Monte Carlo simulation. This double ratio largely cancels experimental and theoretical uncertainties. $R = 1$ is expected if the physics in the Monte Carlo simulation accurately models the data. Several experiments have previously reported significantly low values of R [7, 8, 9].

Neutrino oscillations can explain the observed small values of R . For a two-neutrino mixing hypothesis, the probability for a neutrino produced in flavor state a to be observed in flavor state b after traveling a distance L through a vacuum is:

$$P_{a \rightarrow b} = \sin^2 2\theta \sin^2 \left(\frac{1.27 \Delta m^2 (\text{eV}^2) L (\text{km})}{E_\nu (\text{GeV})} \right), \quad (1)$$

where E_ν is the neutrino energy, θ is the mixing angle between the flavor eigenstates and the mass eigenstates, and Δm^2 is the mass-squared difference of the neutrino mass eigenstates. For detectors near the surface of the Earth, the atmospheric neutrino flight distance, and thus the oscillation probability, is a function of the zenith angle of the neutrino arrival direction. Vertically downward-going neutrinos travel about 15 km while vertically upward-going neutrinos travel about 13,000 km before interacting in the detector. The broad energy spectrum and this range of neutrino flight distances makes measurements of atmospheric neutrinos sensitive to neutrino oscillations with Δm^2 down

to 10^{-4} eV².

In addition to measurements of small values of R both above and below ~ 1 GeV, we observed a significant zenith angle dependent deficit of μ -like events. An exhaustive study of systematic errors in the detector and analysis process, taking into account systematics in the model used in the MC, indicates that no combination of known uncertainties in the experimental measurement or predictions of atmospheric neutrino fluxes is sufficient to explain away our data. In contrast, a two-neutrino oscillation model of $\nu_\mu \leftrightarrow \nu_x$, where ν_x may be ν_τ or a new, non-interacting “sterile” neutrino, is consistent with the observed flavor ratios and zenith angle distributions over the entire energy region.

Up-going muons (UGMs) in Super-K are produced by interactions of atmospheric ν_μ in the rock around the detector. The effective target volume extends outward for many tens of meters into the surrounding rock and increases with the energy of the incoming neutrino, as the high energy muons resulting from these interactions can travel longer distances to reach the detector. Thus, UGMs represent the highest energy portion of the neutrino spectrum observed by Super-Kamiokande, with parent neutrino energy spectra peaking around 10 GeV for stopping muons and 100 GeV for through-going muons. The effective area of the detector is approximately 1250 m² for zenith angle 45°. Currently, limited statistics and larger uncertainties in the expected fluxes make the upward muon data less conclusive than the atmospheric neutrino data, but observations of upward through-going muons and the stopping to through-going ratio as a function of zenith angle are clearly inconsistent with the no-oscillations expectation. Two-flavor oscillations analysis yields allowed regions in $\Delta m^2, \sin^2 2\theta$ consistent with those obtained from the atmospheric neutrino data.

2 Detector

Super-Kamiokande is a cylindrical ring-imaging water Cherenkov detector, with total target mass 50 kilotons, located 1000m underground (2700 mwe overburden)[10]. The detector consists of an inner volume completely surrounded by an optically separated outer veto detector layer. The inner detector volume is 36.2 m high and 33.8 m in diameter, and is lined with 11,146 50 cm diameter photomultiplier tubes (PMT). The outer layer of water is 2.6 – 2.75 m thick and is instrumented with 1885 outward facing 20 cm diameter PMTs. To maximize light collection, a reflective layer of white plastic (Tyvek) covers the walls of the outer detector, and each PMT is fitted with a 60 cm \times 60 cm plate of wavelength shifter. The outer detector is used to reduce background entering

from the surrounding rock and to identify penetrating muons.

A simple hardware trigger based on total collected photoelectrons, presently corresponding to a nominal 4.6 MeV threshold, is used to collect data for solar neutrino analysis; this super-low-energy (SLE) trigger results in a raw trigger rate of 120 Hz, most of which are due to radioactive background near the edges of the detector volume. An online reduction process reduces the rate of recorded events to about 10 Hz. (Earlier data were taken with a nominal 6 MeV threshold and no online reduction, yielding approximately the same recorded data rate.)

An offline data reduction process, which identifies atmospheric neutrino events by applying a higher threshold plus cuts requiring absence of outer detector activity and appropriate hit patterns in the inner detector, yields approximately 9 events per day above a nominal 200 MeV threshold. It is not possible for neutrinos of such high energies to originate in the sun. It is equally improbable that any of these events come from astrophysical sources; a sky map of the high energy event sample shows no significant point sources, and expected astrophysical neutrino fluxes based, for example, on observed gamma ray fluxes, are many orders of magnitude smaller than atmospheric neutrino fluxes in this energy range. We can thus be confident that the observed high energy event sample originates in the upper atmosphere.

Neutrinos are identified by observing final-state leptons produced via charged-current interactions on nuclei, $\nu + N \rightarrow l + X$, with no OD signal consistent with an incoming charged particle. The flavor of the final state lepton is used to identify the flavor of the incoming neutrino. Pattern differences between Cherenkov rings produced by electrons and muons are reflected in a particle identification (PID) parameter which is equivalent to a likelihood ratio. The PID method was tested and verified using KEK charged lepton beams[11].

Events with insignificant OD activity are identified as fully contained (FC). If evidence of outgoing particles is observed in the OD, the event is classified as partially contained (PC). Monte Carlo (MC) studies indicate that PC events are 98.5% ν_μ . Neutrino energy is estimated from the observed total ionization, which for PC events represents a lower limit to the lepton energy.

Events with ID patterns which fit the hypothesis of a single charged muon moving upward, and OD activity consistent with an entering track, are classified as upward-going muons; if OD activity consistent with an exit point is also present, the muon is classified as through-going.

3 Atmospheric Neutrino Data

Super-Kamiokande has collected a total of 4353 FC events and 301 PC events in a 33.0 kiloton-year exposure. For this analysis, the neutrino interaction vertex was required to reconstruct within a 22.5 kiloton fiducial volume, defined to be > 2 m from the ID PMT wall.

FC events were separated into those with a single visible Cherenkov ring and those with multiple Cherenkov rings. For the analysis of FC events, only single-ring events were used. The FC events were further separated into “sub-GeV” ($E_{vis} < 1330$ MeV) and “multi-GeV” ($E_{vis} > 1330$ MeV) samples, where E_{vis} is defined to be the energy of an electron that would produce the observed amount of Cherenkov light. The cut at $E_{vis} = 1330$ MeV, which corresponds to $p_\mu \sim 1400$ MeV/ c , was chosen to allow direct comparison with similarly binned Kamiokande data.

A full-detector Monte Carlo simulation is crucial to the analysis of the data. In the simulation used, a well accepted model[6] was used for atmospheric neutrino production, and detector effects were modelled in detail using GEANT[12]. Exhaustive studies were performed and the detector model was tuned to reflect all available calibration and test data. The MC data are processed by the same reduction software as the real data. For the first 300 live-days of data collected, a separate analysis team developed independent reduction processes, including a separate MC using a different production model[5]. A comparison of results showed no differences within the estimated uncertainties, increasing confidence that there were no significant biases in data selection or event reconstruction algorithms[10, 13]. The data presented here were processed using a merged reduction process.

In a 10-year-equivalent MC sample, 88% (96%) of the sub-GeV e -like (μ -like) events were ν_e (ν_μ) charged-current interactions and 84% (99%) of the multi-GeV e -like (μ -like) events were ν_e (ν_μ) charged-current interactions. All PC events were classified as μ -like, and no single-ring requirement was made. Table 1 summarizes the number of observed events for both data and Monte Carlo as well as the R values for the sub-GeV and multi-GeV samples. Further details of the detector, data selection and event reconstruction used in this analysis are given elsewhere[10, 13].

Super-Kamiokande observes significantly small values of R in both the sub-GeV and multi-GeV samples. Several sources of systematic uncertainties in these measurements have been considered.

Cosmic ray induced interactions in the rock surrounding the detector could provide a

	Data	Monte Carlo
<hr/>		
sub-GeV		
single-ring	2389	2622.6
<i>e</i> -like	1231	1049.1
<i>μ</i> -like	1158	1573.6
multi-ring	911	980.7
<hr/>		
total	3300	3603.3
	$R = 0.63 \pm 0.03 (stat.) \pm 0.05 (sys.)$	
<hr/> <hr/>		
multi-GeV		
single-ring	520	531.7
<i>e</i> -like	290	236.0
<i>μ</i> -like	230	295.7
multi-ring	533	560.1
<hr/>		
total	1053	1091.8
<hr/>		
partially-contained	301	371.6
	$R_{FC+PC} = 0.65 \pm 0.05 (stat.) \pm 0.08 (sys.)$	

Table 1: Summary of the sub-GeV, multi-GeV and PC event samples compared with the Monte Carlo prediction based on the neutrino flux calculation of Honda *et al*[6].

source of e -like contamination from neutrons [14], but Super-Kamiokande has 4.7 meters of water surrounding the fiducial volume; this distance corresponds to roughly 5 hadronic interaction lengths and 13 radiation lengths[15]. Event vertex distributions show no excess of e -like events close to the fiducial boundary[10, 13].

The prediction of the ratio of the ν_μ flux to the ν_e flux is dominated by the well-understood decay chain of mesons and contributes less than 5% to the uncertainty in R . Different neutrino flux models vary by about $\pm 20\%$ in predicted absolute rates, but the ratio is robust[16]. Uncertainties in R due to a difference in cross sections for ν_e and ν_μ have been studied[17]; however, lepton universality prevents any significant difference in cross-sections at energies much above the muon mass and thus errors in cross-sections could not produce a small value of R in the multi-GeV energy range. Particle identification was estimated to be $\gtrsim 98\%$ efficient for both μ -like and e -like events based on Monte Carlo studies. Particle identification was also tested in Super-Kamiokande using Michel electrons and stopping cosmic-ray muons, and the μ -like and e -like events used in this analysis are clearly separated[10].

Other explanations for the small value of R , such as contributions from nucleon decays [18], can be discounted as they would not display the zenith angle effects described below.

We estimate the probability that the observed μ/e ratios could be due to statistical fluctuation is less than 0.001% for sub-GeV R and less than 1% for multi-GeV R .

The μ -like data exhibit a clear asymmetry in zenith angle (Θ) while no significant asymmetry is observed in the e -like data [13]. The asymmetry may be defined as $A = (U - D)/(U + D)$ where U is the number of upward-going events ($-1 < \cos \Theta < -0.2$) and D is the number of downward-going events ($0.2 < \cos \Theta < 1$). A is expected to be near zero independent of flux model for $E_\nu > 1$ GeV, above which effects due to the Earth's magnetic field on cosmic rays are small. Treatment of geomagnetic effects results in an uncertainty of roughly ± 0.02 in the expected asymmetry of e -like and μ -like sub-GeV events and less than ± 0.01 for multi-GeV events. Studies of decay electrons from stopping muons show at most a $\pm 0.6\%$ up-down difference in Cherenkov light detection[19].

Figure 1 shows A as a function of momentum for both e -like and μ -like events. In the present data, the asymmetry as a function of momentum for e -like events is consistent with expectations, while the μ -like asymmetry at low momentum is consistent with zero but significantly deviates from expectation at higher momentum. The average angle between the final state lepton direction and the incoming neutrino direction is 55° at $p = 400$ MeV/ c and 20° at 1.5 GeV/ c . At the lower momenta in Fig. 1, the possible asymmetry

of the neutrino flux is largely washed out. We have found no detector bias differentiating e -like and μ -like events that could explain an asymmetry in μ -like events but not in e -like events [13].

Considering multi-GeV (FC+PC) muons alone, the measured asymmetry, $A = -0.296 \pm 0.048 \pm 0.01$ deviates from zero by more than 6 standard deviations.

4 Upward Muon Data

The flux of surviving cosmic ray muons in the downward direction (downward-going muons, DGMs) is overwhelming compared to down-going neutrino-induced muons (2.2 Hz DGM's as compared with ~ 1.5 neutrino-induced muons per day). While this background cuts off sharply at $\theta_Z > 90^\circ$, tracking angular resolution and multiple Coulomb scattering make DGMs a significant background for UGMs with $\cos(\theta_Z)$ close to zero. The contribution of DGM's to the UGM data in the zenith angle bin closest to the horizon has been estimated by comparing regions in azimuth near the horizon with different rock overburdens.

Events are required to have ≥ 7 meters measured path length ($E_\mu > 1.6$ GeV) in the inner detector fiducial volume. The angular and track length resolution were determined to be $\sim 1^\circ$ and $\sim 6\%$ by fitting monte carlo events. Taking into account the known overburden profile, and making appropriate corrections for near-horizontal DGM leakage into the first UGM zenith angle bin, we obtain the through-going UGM zenith angle distributions shown in Figure 5. Also shown are distributions expected assuming no oscillations, and assuming values of oscillation parameters consistent with those obtained from the Super-K atmospheric neutrino data analysis and the Kamiokande allowed region ($\sin^2(2\theta) = 1.0$, $\Delta m^2 = 0.005$ eV²). The data are summarized in Table 2.

Predicted values were obtained using methods similar to those described by Lipari *et al*[20], including deep-inelastic, quasi-elastic, and π production interaction channels. The theoretical absolute flux is uncertain by $\sim 20\%$, but the shape of the zenith angle distribution is known to $\sim 5\%$.

Systematic uncertainties in the predicted values for both through-going and stopping muon fluxes limit their ability to provide conclusive evidence for or against neutrino oscillations. However, as with the atmospheric neutrino data, common systematics are canceled by taking a ratio: in this case, the ratio of stopping to through-going UGMs (\mathfrak{R}). The resulting error on the ratio is $\sim 14\%$, and is due primarily to uncertainty in the

Table 2: Super-Kamiokande Upward-Going Muon Data Summary (predictions are for the case of no ν oscillations)

	Through-going	Stopping
Events	617	137
DGM background ($\cos \theta_Z > -0.10$)	4.6	13.2
Net flux Φ_{DATA} ($\times 10^{-13} cm^{-2} s^{-1} sr^{-1}$)	$1.75 \pm 0.07(stat) \pm 0.08(syst)$	$0.38 \pm 0.04(stat)_{-0.02}^{+0.03}(syst)$
Predicted flux Φ_{PRED} ($\times 10^{-13} cm^{-2} s^{-1} sr^{-1}$)	1.88 ± 0.38	0.73 ± 0.15
Stop/through ratio		
$\mathfrak{R} = \Phi_{STOP}/\Phi_{THRU}$	$0.217 \pm 0.023(stat)_{-0.013}^{+0.014}(syst)$	
Predicted \mathfrak{R}	$0.388_{-0.047}^{+0.052}$	

cosmic ray spectral index. Furthermore, the parent neutrino energy spectra indicate that, for $\sin^2(2\theta) = 1.0$, $\Delta m^2 \sim 0.005 eV^2$, with $\langle L_\nu \rangle = 6000$ km, the probability of oscillation becomes negligible for energies above about 40 GeV, where through-going muons begin to dominate the UGM flux. Thus we expect the ratio of stopping/through-going fluxes to decrease in the presence of flavor oscillations. This effect is apparent in Figure 6, which shows the stop/through ratio, along with no-oscillation and oscillation predictions as in Figure 5.

5 Oscillations Analysis

We examined the hypotheses of two-flavor $\nu_\mu \leftrightarrow \nu_e$ and $\nu_\mu \leftrightarrow \nu_\tau$ oscillation models using a χ^2 comparison of data and Monte Carlo, allowing all important Monte Carlo parameters to vary, weighted by their expected uncertainties.

The data were binned by particle type, momentum, and $\cos \Theta$. A χ^2 was defined as:

$$\chi^2 = \sum_{\cos \Theta, p} (N_{DATA} - N_{MC})^2 / \sigma^2 + \sum_j \epsilon_j^2 / \sigma_j^2, \quad (2)$$

where the sum is over five bins equally spaced in $\cos \Theta$ and seven momentum bins for both e -like events and μ -like plus PC events (70 bins total). The statistical error, σ ,

accounts for both data statistics and the weighted Monte Carlo statistics. N_{DATA} is the measured number of events in each bin. N_{MC} is the weighted sum of Monte Carlo events:

$$N_{MC} = \frac{\mathcal{L}_{DATA}}{\mathcal{L}_{MC}} \times \sum_{\text{MC events}} w(\alpha, \epsilon_j). \quad (3)$$

\mathcal{L}_{DATA} and \mathcal{L}_{MC} are the data and Monte Carlo live-times. For each Monte Carlo event, the weight w depends upon E_ν , $\cos \Theta$ (*i.e.*, L) and the values of oscillation parameters ($\sin^2 2\theta, \Delta m^2$) considered, as well as the Monte Carlo fit parameters, α and $\epsilon_j \equiv (\beta_s, \beta_m, \delta, \rho, \lambda, \eta_s, \eta_m)$, which are summarized in Table 3 along with their estimated uncertainties, σ_j . The over-all normalization, α , was allowed to vary freely. A global scan was made on a $(\sin^2 2\theta, \log \Delta m^2)$ grid minimizing χ^2 with respect to the fit parameters α, ϵ_j at each point. Details of the fitting procedure are given in Ref. [2].

The oscillation simulations used profiles of neutrino production heights calculated in Ref. [21], which account for the competing factors of production, propagation, and decay of muons and mesons through the atmosphere. For $\nu_\mu \leftrightarrow \nu_e$, effects of matter on neutrino propagation through the Earth were included following Ref. [22, 23]. Due to the small number of events expected from τ -production, the effects of τ appearance and decay were neglected in simulations of $\nu_\mu \leftrightarrow \nu_\tau$.

The best-fit to $\nu_\mu \leftrightarrow \nu_\tau$ oscillations, $\chi^2_{min} = 65.2/67$ DOF, was obtained at ($\sin^2 2\theta = 1.0, \Delta m^2 = 2.2 \times 10^{-3}$ eV²) inside the physical region ($0 \leq \sin^2 2\theta \leq 1$). The best-fit values of the Monte Carlo parameters (summarized in Table 3) were all within their expected errors. The global minimum occurred slightly outside the physical region at ($\sin^2 2\theta = 1.05, \Delta m^2 = 2.2 \times 10^{-3}$ eV², $\chi^2_{min} = 64.8/67$ DOF). The contours of the 68%, 90% and 99% confidence intervals are located at $\chi^2_{min} + 2.6, 5.0$, and 9.6 based on the minimum inside the physical region[24]. These contours are shown in Fig. 2. The region near χ^2 minimum is rather flat and has many local minima so that inside the 68% interval the best-fit Δm^2 is not well constrained. Outside the 99% allowed region the χ^2 increases rapidly.

In contrast, we obtained a poor fit, $\chi^2 = 135/69$ DOF, for $\sin^2 2\theta = 0, \Delta m^2 = 0$ (*i.e.* assuming no oscillations). Similarly, for $\nu_\mu \leftrightarrow \nu_e$ oscillations, we obtained a relatively poor minimum: $\chi^2_{min} = 87.8/67$ DOF, at ($\sin^2 2\theta = 0.93, \Delta m^2 = 3.2 \times 10^{-3}$ eV²).

The expected asymmetry of the multi-GeV e -like events for the best-fit $\nu_\mu \leftrightarrow \nu_e$ oscillation hypothesis, $A = 0.205$, differs from the measured asymmetry, $A = -0.036 \pm 0.067 \pm 0.02$, by 3.4 standard deviations. We conclude that the $\nu_\mu \leftrightarrow \nu_e$ hypothesis is not favored.

	Monte Carlo Fit Parameters	Best Fit	Uncertainty
α	overall normalization	15.8%	(*)
δ	E_ν spectral index	0.006	$\sigma_\delta = 0.05$
β_s	sub-GeV μ/e ratio	-6.3%	$\sigma_s = 8\%$
β_m	multi-GeV μ/e ratio	-11.8%	$\sigma_m = 12\%$
ρ	relative norm. of PC to FC	-1.8%	$\sigma_\rho = 8\%$
λ	L/E_ν	3.1%	$\sigma_\lambda = 15\%$
η_s	sub-GeV up-down	2.4%	$\sigma_\eta^s = 2.4\%$
η_m	multi-GeV up-down	-0.09%	$\sigma_\eta^m = 2.7\%$

Table 3: Summary of Monte Carlo fit parameters. Best-fit values for $\nu_\mu \leftrightarrow \nu_\tau$ ($\Delta m^2 = 2.2 \times 10^{-3} \text{eV}^2$, $\sin^2 2\theta = 1.0$) and estimated uncertainties are given. (*)The over-all normalization (α) was estimated to have a 25% uncertainty but was fitted as a free parameter.

The zenith angle distributions for the FC and PC samples are shown in Fig. 3. The data are compared to the Monte Carlo expectation (no oscillations, hatched region) and the best-fit expectation for $\nu_\mu \leftrightarrow \nu_\tau$ oscillations (bold line).

We also estimated the oscillation parameters considering the R measurement and the zenith angle shape separately. The 90% confidence level allowed regions for each case overlapped at $1 \times 10^{-3} < \Delta m^2 < 4 \times 10^{-3} \text{eV}^2$ for $\sin^2 2\theta = 1$.

As a cross-check of the above analyses, we have reconstructed the best estimate of the ratio L/E_ν for each event. The neutrino energy is estimated by applying a correction to the final state lepton momentum. Typically, final state leptons with $p \sim 100 \text{MeV}/c$ carry 65% of the incoming neutrino energy increasing to $\sim 85\%$ at $p = 1 \text{GeV}/c$. The neutrino flight distance L is estimated following Ref. [21] using the estimated neutrino energy and the reconstructed lepton direction and flavor. Figure 4 shows the ratio of FC data to Monte Carlo for e -like and μ -like events with $p > 400 \text{MeV}/c$ as a function of L/E_ν , compared to the expectation for $\nu_\mu \leftrightarrow \nu_\tau$ oscillations with our best-fit parameters. The e -like data show no significant variation in L/E_ν , while the μ -like events show a significant deficit at large L/E_ν . At large L/E_ν , the ν_μ have presumably undergone numerous oscillations and have averaged out to roughly half the initial rate.

For the upward-going muon data, allowed regions for oscillation parameters were determined from fits to the through-going muon distribution shown in Figure 5 and the stopping/through ratio shown in Figure 6, compared to oscillation predictions calculated

at a grid of points in oscillation parameter space. Procedures used were similar to those described above for the atmospheric neutrino analysis.

Fits for each test point in oscillation parameter space $\sin^2(2\theta), \Delta m^2$ were performed by minimizing

$$\chi^2 = \sum_{bin=1}^{10} \left(\frac{\Phi_{data}(bin) - \alpha \Phi_{theo}(bin)}{\sigma_{data}(bin)} \right)^2 + \left(\frac{1 - \alpha}{\sigma_\alpha} \right)^2$$

where α is the absolute flux normalization, with $\sigma_\alpha = 20\%$.

Similarly, fits to \mathfrak{R} as a function of oscillation parameters were performed by minimizing

$$\chi^2 = \sum_{bin=1}^5 \left(\frac{\mathfrak{R}_{data}(bin) - \eta \mathfrak{R}_{theo}(bin)}{\sigma_{data}(bin)} \right)^2 + \left(\frac{1 - \eta}{\sigma_\eta} \right)^2$$

where η is the \mathfrak{R} normalization, with $\sigma_\eta \simeq 14\%$.

α and η were minimized at each point in parameter space. The unphysical region was taken into account when calculating the probability contours. The allowed regions obtained are consistent with those obtained from analysis atmospheric neutrino data (Figure 7). These results are interpreted as independent evidence for neutrino oscillations for several reasons. The shape of the through-going UGM flux zenith angle distribution is inconsistent with the no-oscillation prediction ($\chi^2 = 18.3$ for 9 degrees of freedom, a probability of $\sim 2\%$). The stop/through ratio \mathfrak{R} as a function of zenith angle for the no-oscillation case is also improbable (\mathfrak{R}_{data} differs from \mathfrak{R}_{theo} by 3.2σ , a probability of $< 1\%$). However, parameter estimation in $\sin^2(2\theta), \Delta m^2$ space shows that $\nu_\mu \rightarrow \nu_\tau$ oscillations with maximal mixing and Δm^2 in the range of $\sim 7 \times 10^{-4} \text{ eV}^2$ to $\sim 2 \times 10^{-2} \text{ eV}^2$ are consistent with the observed data.

6 Conclusions

The asymmetry A of the e -like events in the present data is consistent with expectation in the absence of neutrino oscillations and two-flavor $\nu_e \leftrightarrow \nu_\mu$ oscillations are not favored. This is in agreement with recent results from the CHOOZ experiment[25]. The LSND experiment has reported the appearance of ν_e in a beam of ν_μ produced by stopped pions[26]. The LSND results do not contradict the present results if they are observing small mixing angles. With the best-fit parameters for $\nu_\mu \leftrightarrow \nu_\tau$ oscillations, we expect a total of only 15-20 events from ν_τ charged-current interactions in the data sample. Using

the current sample, oscillations between ν_μ and ν_τ are indistinguishable from oscillations between ν_μ and a non-interacting “sterile” neutrino.

Figure 2 shows the Super–Kamiokande results overlaid with the allowed region obtained by the Kamiokande experiment[27]. The Super–Kamiokande region favors lower values of Δm^2 than allowed by the Kamiokande experiment; however the 90% contours from both experiments have a region of overlap.

Both the zenith angle distribution of μ -like events and the value of R observed in this experiment significantly differ from the best predictions in the absence of neutrino oscillations. While uncertainties in the flux prediction, cross sections, and experimental biases are ruled out as explanations of the observations, the present data are in good agreement with two-flavor $\nu_\mu \leftrightarrow \nu_\tau$ oscillations with $\sin^2 2\theta > 0.82$ and $5 \times 10^{-4} < \Delta m^2 < 6 \times 10^{-3} \text{ eV}^2$ at 90% confidence level.

Preliminary studies of upward-going stopping and through-going muons in Super–Kamiokande[3] confirm the conclusions obtained from the atmospheric neutrino analysis. The angular distributions differ significantly from the predictions of the no-oscillations hypothesis, and an oscillations analysis gives allowed regions consistent with the atmospheric neutrino results. MACRO[28] has recently reported very similar results.

We conclude that the present data give internally consistent evidence for neutrino oscillations. Detector operation continues with $> 95\%$ livetime efficiency, and intensive effort to improve predictions for upward-going muons using a new monte carlo is underway.

I wish to thank Prof. Bellettini for the opportunity to attend a truly wonderful conference, and Prof. Greco for his patience regarding this paper. Thanks are also due to many Super–Kamiokandecollaborators for help preparing this paper; any errors introduced are mine alone. We gratefully acknowledge the cooperation of the Kamioka Mining and Smelting Company. The Super–Kamiokande experiment was built and has been operated with funding from the Japanese Ministry of Education, Science, Sports and Culture, and the United States Department of Energy.

References

- [1] See ref. 2 below for a complete list of Super–Kamiokande Collaboration members.
- [2] The Super-Kamiokande Collaboration, Y. Fukuda, *et al.*, Phys. Rev. Lett. **81**, 1562 (1998).

- [3] T. Kajita, to be published in Proceedings of the XVIIIth International Conference on Neutrino Physics and Astrophysics, Takayama, Japan, June, 1998.
- [4] A. Habig and M. Yoshida, poster paper at the XVIIIth International Conference on Neutrino Physics and Astrophysics, Takayama, Japan, June 1998.
- [5] G. Barr *et al.*, Phys. Rev. **D39**, 3532 (1989); V. Agrawal, *et al.*, Phys. Rev. **D53**, 1313 (1996); T. K. Gaisser and T. Stanev, Proc. 24th Int. Cosmic Ray Conf. (Rome) Vol. 1 694 (1995).
- [6] M. Honda *et al.*, Phys. Lett. **B248**, 193 (1990); M. Honda *et al.*, Phys. Lett. **D52**, 4985 (1995).
- [7] K.S. Hirata *et al.*, Phys. Lett. **B205**, 416 (1988); K.S. Hirata *et al.*, Phys. Lett. **B280**, 146 (1992).
- [8] D. Casper, *et al.*, Phys. Rev. Lett. **66**, 2561 (1991); R. Becker-Szendy *et al.*, Phys. Rev. **D46**, 3720 (1992).
- [9] W.W.M. Allison *et al.*, Phys. Lett. **B391**, 491 (1997); T. Kafka, proceedings of 5th Int. Workshop on Topics in Astroparticle and Underground Physics, Gran Sasso, Italy, Sep. 1997.
- [10] Super-Kamiokande Collaboration, Y. Fukuda, *et al.*, Phys. Lett. **B433**, 9 (1998).
- [11] S. Kasuga, *et al.*, Phys. Lett. **B374**, 238 (1996).
- [12] CERN Program Library, Long Writeup W5013, 1993.
- [13] Super-Kamiokande Collaboration, Y. Fukuda, *et al.*, to be published in Phys. Lett. B, see preprint hep-ex/9805006.
- [14] O.G. Ryazhskaya, JETP Lett. **60**, 617 (1994); JETP Lett. **61**, 237 (1995).
- [15] Y. Fukuda, *et al.*, Phys. Lett. **B388**, 397 (1996).
- [16] T. K. Gaisser *et al.*, Phys. Rev. **D54**, 5578 (1996)
- [17] J. Engel *et al.*, Phys. Rev. **D48**, (1993) 3048.
- [18] W.A. Mann, T. Kafka and W. Leeson, Phys. Lett. **B291**, 200 (1992).

- [19] This represents an improvement from Refs.[10, 13] due to improved calibration. See The Super-Kamiokande Collaboration, “Calibration of Super-Kamiokande Using an Electron Linac”, preprint hep-ex/9807027; submitted to NIM A.
- [20] Lipari, P. *et al* 1994, Phys.Rev.Lett. 74, 4384.
- [21] T. K. Gaisser and T. Stanev, Phys. Rev. **D57**, 1977 (1998).
- [22] L. Wolfenstein, Phys. Rev. **D17**, 2369 (1978).
- [23] S. P. Mikheyev and A. Y. Smirnov, Sov. J. Nucl. Phys. **42**, 1441 (1985); S. P. Mikheyev and A. Y. Smirnov, Nuovo Cim. **9C**, 17 (1986); S. P. Mikheyev and A. Y. Smirnov, Sov. Phys. Usp. **30**, 759 (1987).
- [24] Based on a two-dimensional extension of the method from the Particle Data Group, Review of Particle Physics, Section: Errors and confidence intervals – Bounded physical region, June 1996: R.M. Barnett *et al.* Phys. Rev. **D54**, 375 (1996).
- [25] M. Apollonio *et al.*, Phys. Lett. **B420** 397 (1998)
- [26] C. Athanassopoulos, *et al.*, Phys. Rev. C **54**, 2685 (1996); Phys. Rev. Lett. **77**, 3082 (1996).
- [27] Y. Fukuda *et al.*, Phys. Lett. **B335**, 237 (1994).
- [28] M. Ambrosio, *et al.*, submitted to Phys. Lett. (preprint hep-ex/9807005).

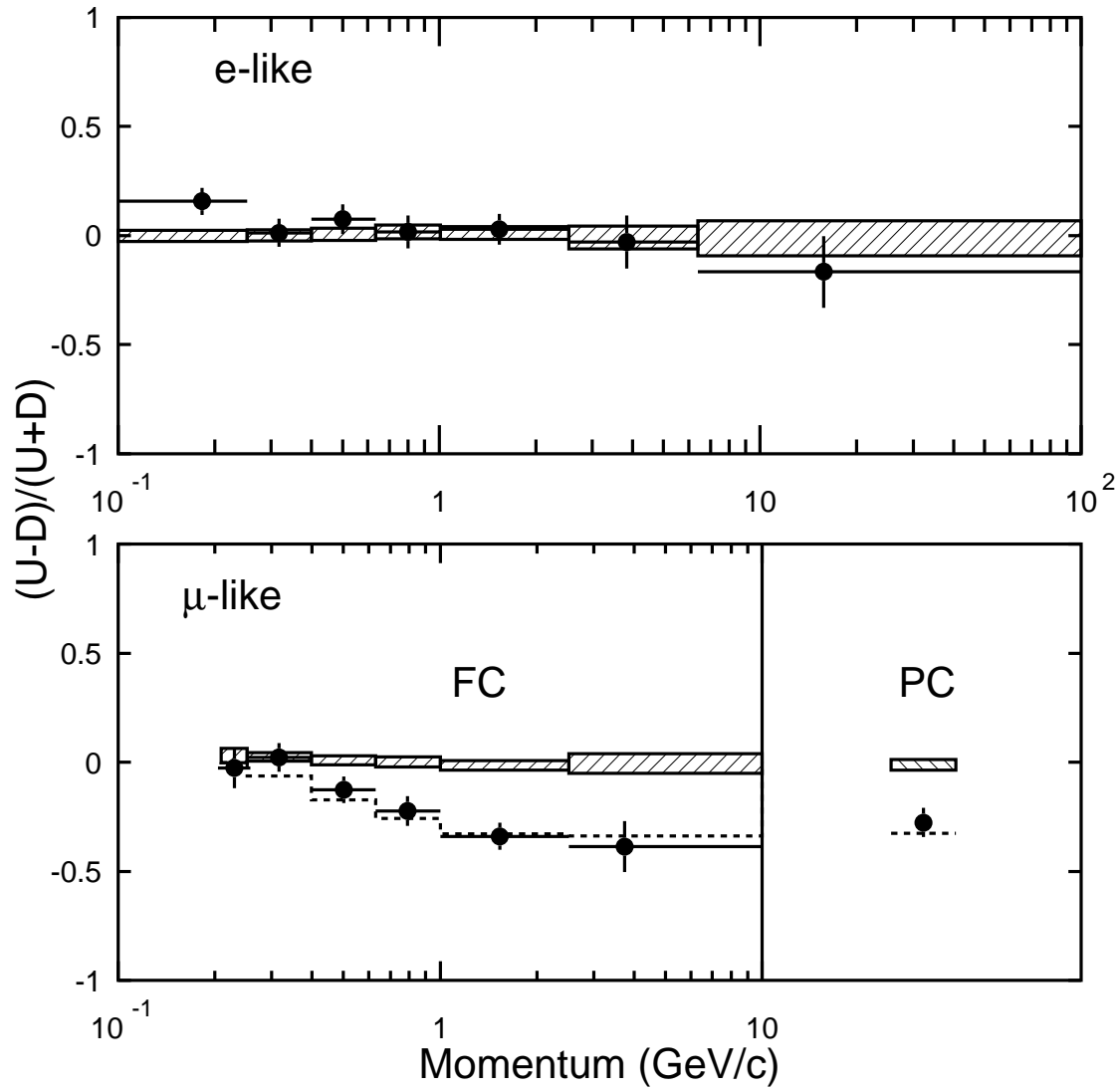


Figure 1: Asymmetry parameter ($A = (U - D)/(U + D)$, where U is the number of upward-going events and D is the number of downward-going events) vs momentum.

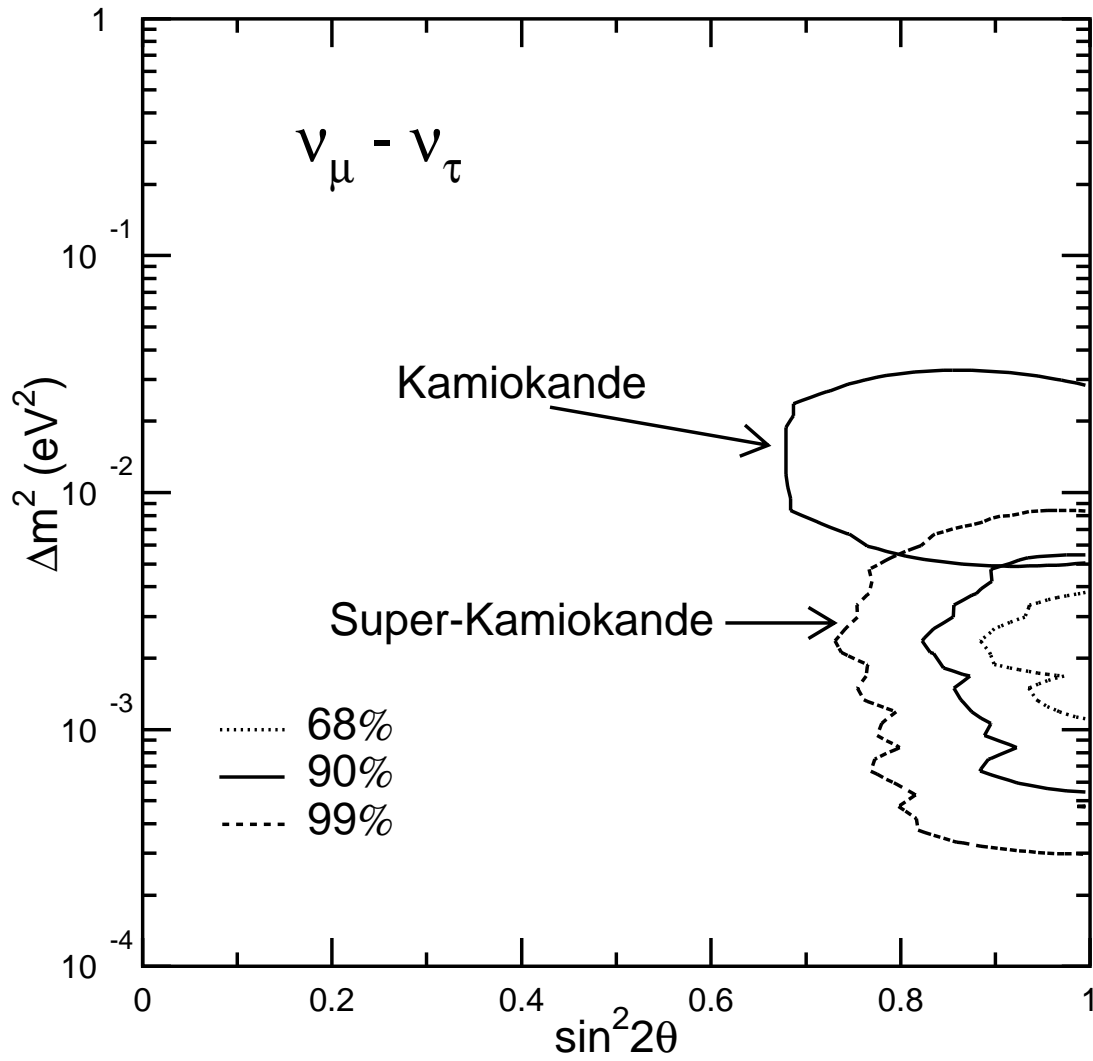


Figure 2: Allowed region in oscillation parameter space from atmospheric neutrino data (68%, 90% and 99% contours shown). Also shown is allowed region reported by Kamiokande.

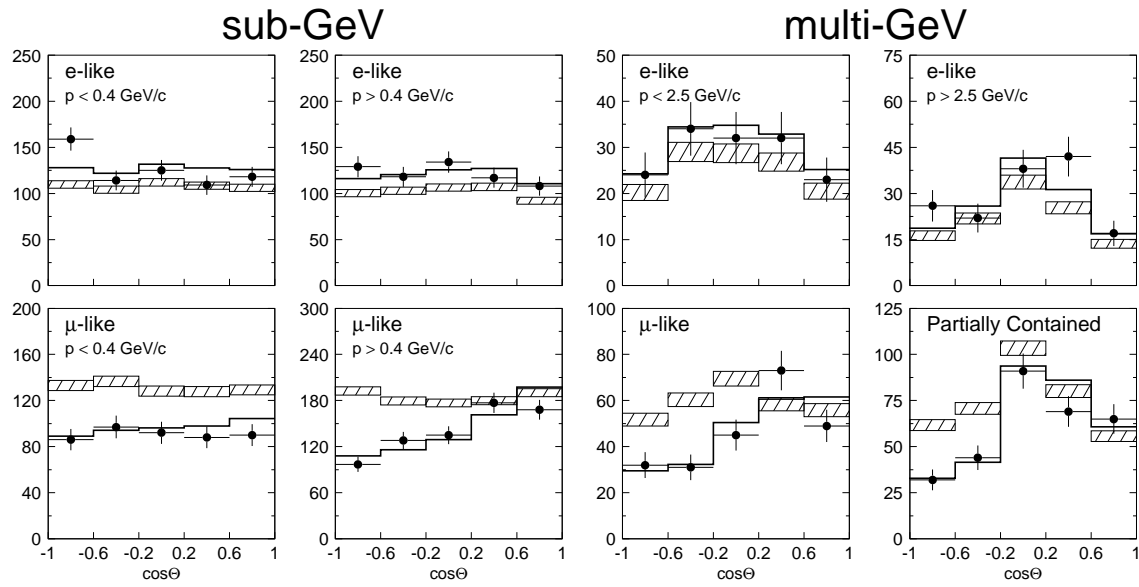


Figure 3: Angular distributions for e-like and μ -like atmospheric neutrino events. Solid and dashed lines show expected values for no-oscillation case, and best-fit oscillation parameters, respectively.

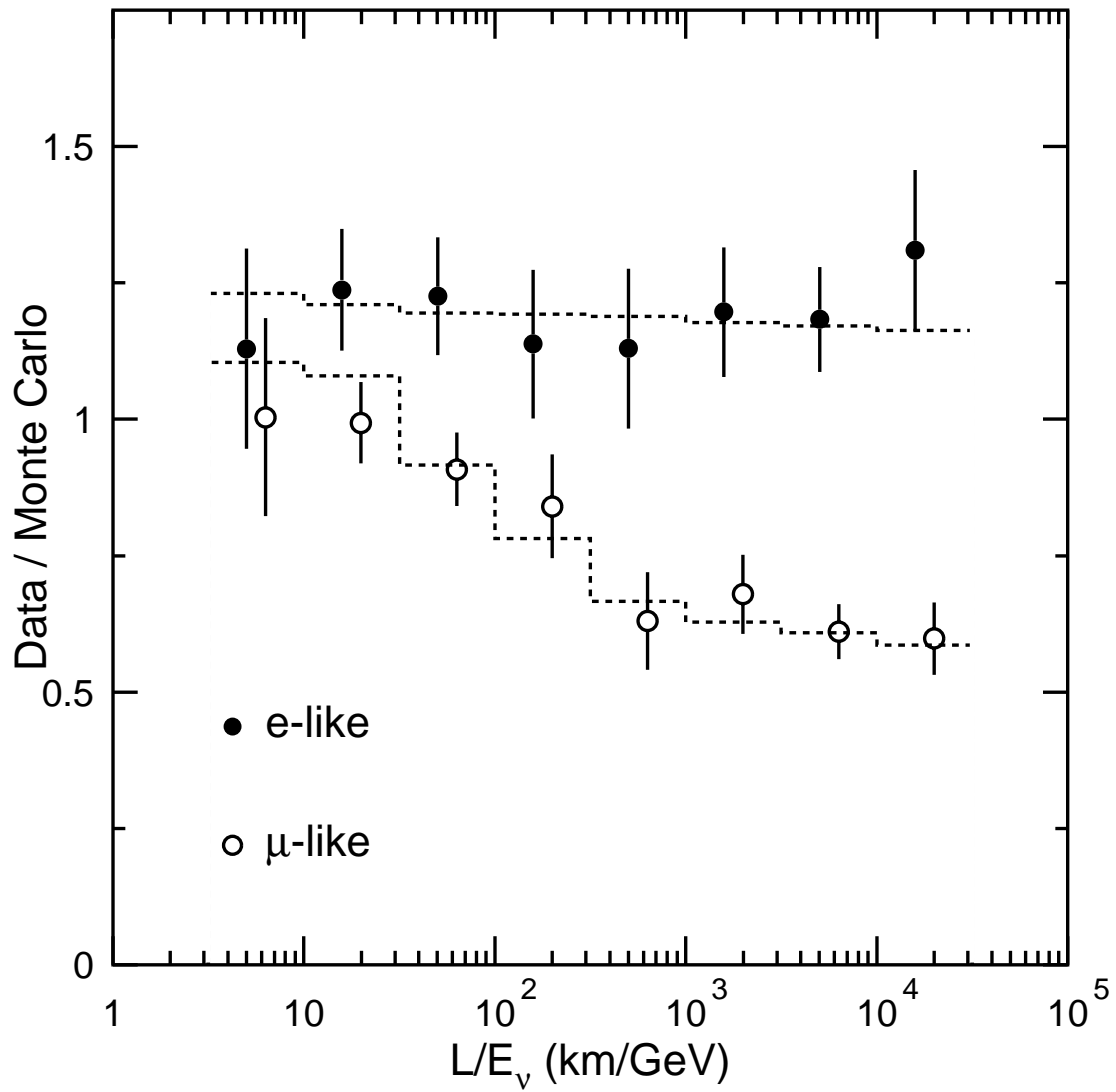


Figure 4: Momentum distribution of L/E for atmospheric neutrinos, with dashed curve showing expectation for best-fit oscillation parameters.

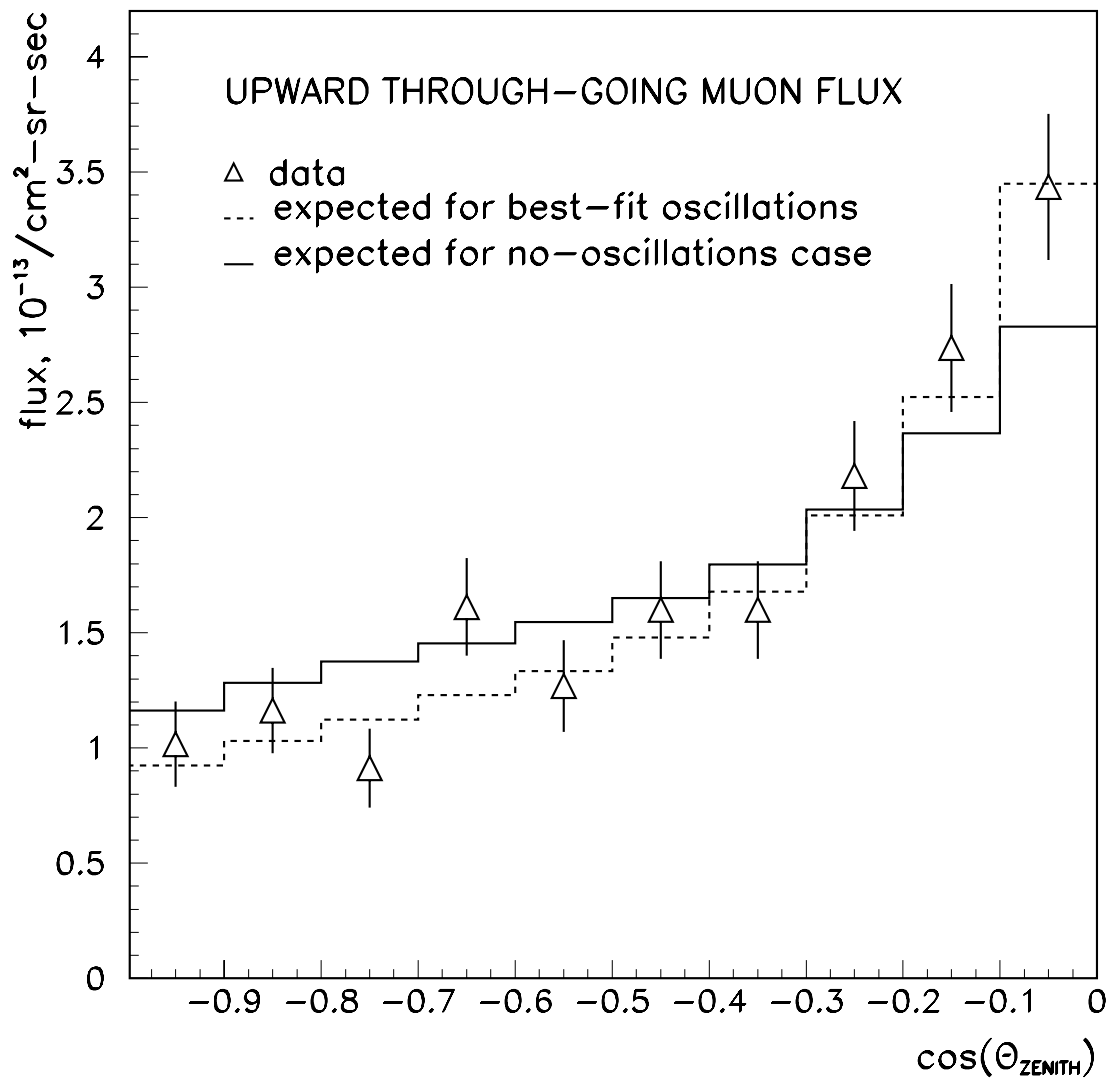


Figure 5: Through-going upward muons vs zenith angle

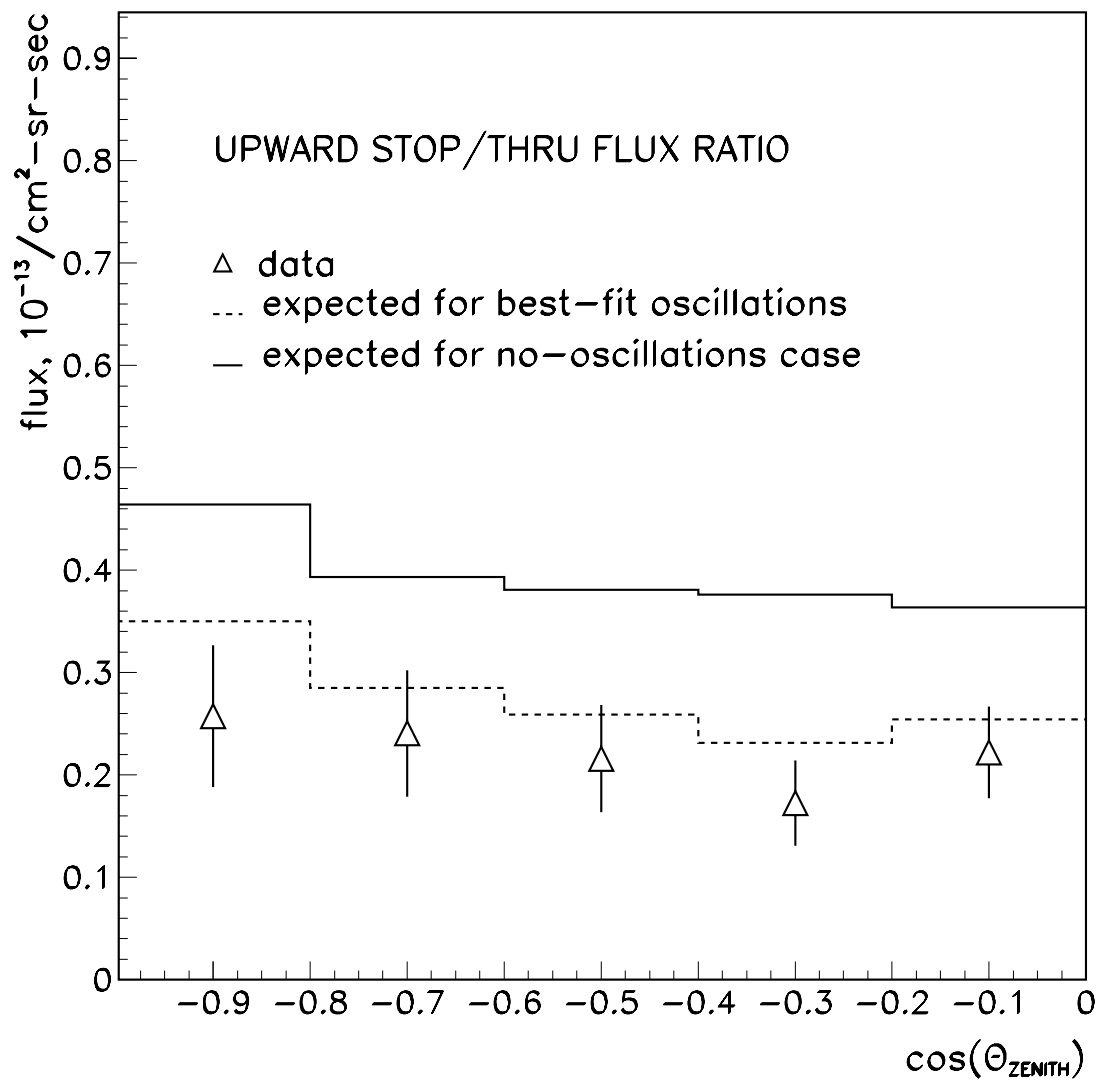


Figure 6: Stop/Through Ratio vs zenith angle

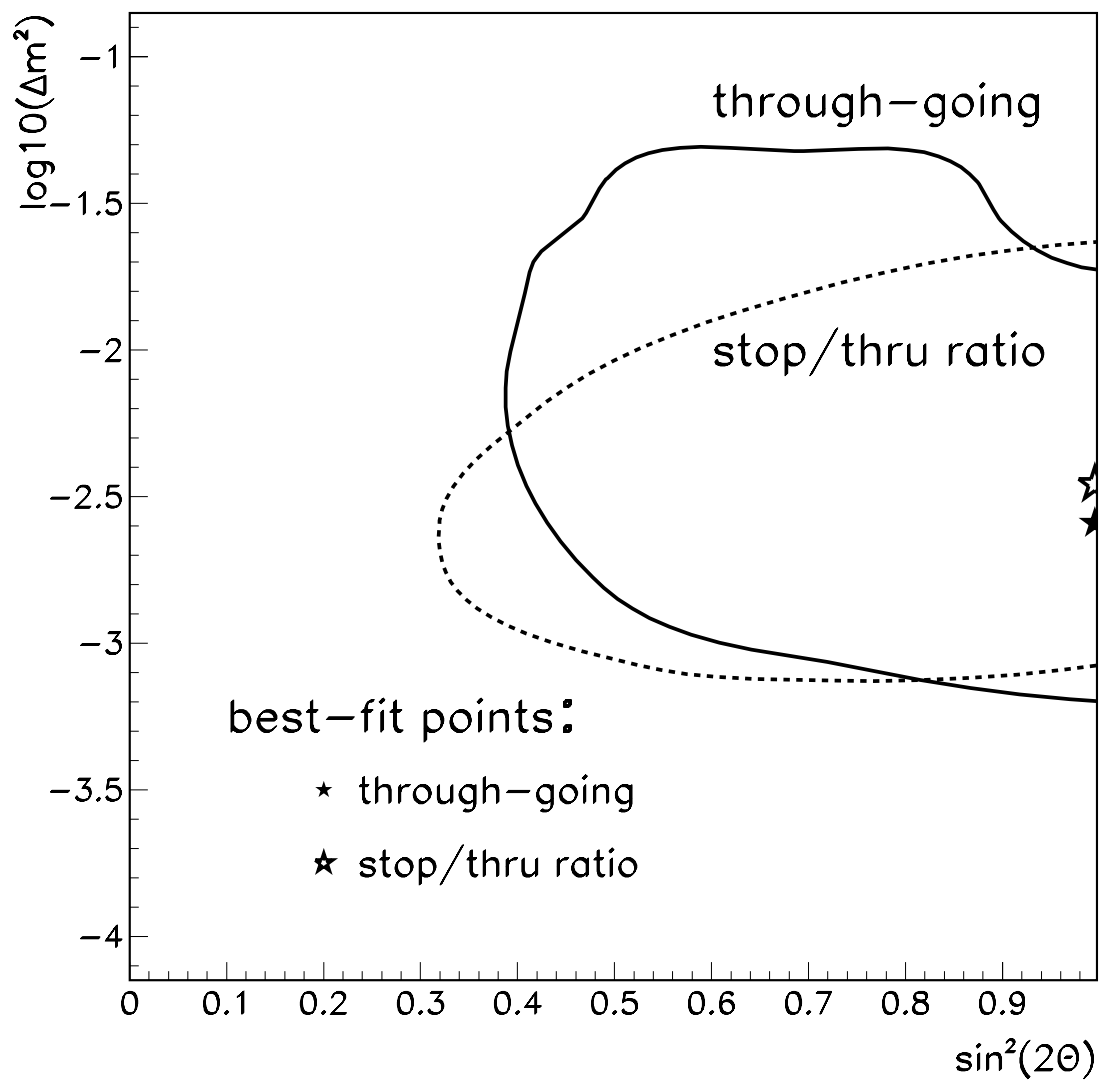


Figure 7: Allowed regions from upward-going muon data